On the potential of connected stars as auxetic systems

Joseph N Grima, Ruben Gatt, Andrew Alderson, Kenneth Evans

On the potential of connected stars as auxetic systems

Note: The following files were submitted by the author for peer review, but cannot be converted to PDF. You must view these files (e.g. movies) online.

Fig4a__STAR3_ka50_kb50.gif
Fig4b__STAR3_ka800_kb50.gif
Fig4c__STAR3_ka50_kb800.gif
Fig4d__STAR3_ka800_kb800.gif
Fig5a__STAR4_ka50_kb50.gif
Fig5b__STAR4_ka800_kb50.gif
Fig5c__STAR4_ka50_kb800.gif
Fig5d__STAR4_ka800_kb800.gif
Fig6a__STAR6_ka50_kb50.gif
Fig6b__STAR6_ka800_kb50.gif
Fig6c__STAR6_ka50_kb800.gif
Fig6d__STAR6_ka800_kb800.gif

SCHOLARONE™
Manuscripts

1
2
3
4
5
6
7
8
9
10
11
12
13
14
15
16
17
18
19
20
21
22
23
24
25
26
27
28
29
30
31
32
33
34
35
36
37
38
39
40
41
42
43
44
45
46
47
48
49
50
51
52
53
54
55
56
57
58
59
60

On the potential of connected stars as auxetic systems

JOSEPH N. GRIMA*[†], RUBEN GATT[†], ANDREW ALDERSON[‡]

and KENNETH E. EVANS[¶]

[†] Department of Chemistry, University of Malta, Msida, MSD 05, Malta

e-mail: joseph.grima@um.edu.mt - www: http://home.um.edu.mt/auxetic

[‡] Centre for Materials Research and Innovation, University of Bolton, Bolton, BL3 5AB, UK

[¶] Department of Engineering, University of Exeter, Exeter, EX4 4QF, UK.

Auxetic materials and structures exhibit the unexpected

behaviour of getting wider when stretched and thinner when

compressed. This behaviour requires the structures (the internal

structure in the case of materials) to have geometric features which

must deform in a way that results in the structure expanding when

stretched. This paper assesses the potential for auxetic behaviour of a

novel class of two-dimensional periodic structures which can be

described as 'connected stars' as they contain star-shaped units of

different rotational symmetry which are connected together to form

two-dimensional periodic structures. These structures will be studied

through a technique based on force-field based methods (the EMUDA

technique) and it will be shown that some, but not all, of these

structures can exhibit auxetic behaviour. An attempt is made to explain

the reasons for the presence or absence of a negative Poisson's ratio in

these systems.

Keywords: Auxetic; negative Poisson's ratio; stars; modelling; EMUDA

2

1. Introduction

Auxetic materials [1] (i.e. materials with a negative Poisson's ratio) exhibit the unexpected behaviour of getting fatter when stretched and thinner when compressed. In recent years, auxetic behaviour has been experimentally measured or predicted in various types of materials including foams [2 - 7], nanostructured and liquid crystalline polymers [1, 8 - 12], microstructured polymers [13 - 15], cubic metals [16], silicates [17 - 22] and zeolites [23]. In all of these materials, the auxetic effect arises from the geometry of the nanostructure or microstructure of these materials and the way this deforms when subjected to uniaxial loads (deformation mechanism) [24]. It has also been shown that the Poisson's ratio is a scale-independent property, i.e. the deformation mechanism can operate at any scale ranging form the nano-level (molecular level) to the macroscale. In fact, in some cases, the same 'deformation mechanism' has been used to explain the presence of auxetic behaviour in very different systems. For example, the 'rotation of rigid units' model has been used to account for the auxetic behaviour in materials ranging from silicates and zeolites (where the auxetic effect is due to nanostructure of the materials) [22, 23] to polymeric foams (where the auxetic effect is due to features at the micro-millimetre scale) [7] and macrostructures [26].

The scale-independence of the Poisson's ratios offers the possibility to classify auxetics according to the type of 'geometry / deformation mechanism' that givers rise to the auxetic behaviour. Such a classification simplifies the study of auxetics as it allows the formulation of theories and explanations that can be applied to materials at various scales. As a consequence of this, an approach for studying auxetic systems is to study 'idealised structures' (in particular, two or three dimensional periodic

macrostructures) which expand when stretched. These 'structures', apart from being interesting in their own accord, provide researchers with useful information on which structural features may be implemented at the micro / nano level to produce auxetic materials which mimic the behaviour of these 'macrostructures'.

There are various techniques that can be used to study the properties (including the potential as auxetics) of structures, ranging from (i) the construction of real physical models which can be mechanically tested, to, (ii) the derivation of analytical expressions which describe the 'mechanical properties' of the structures in terms of various geometric and structural parameters. In this respect, we have recently proposed a new methodology for performing such studies where structures are constructed within standard molecular modelling packages using 'dummy atoms' and modelled using a force-field based energy expression which contains bond terms but no non-bond terms [26]. This new technique of 'empirical modelling using dummy atoms' (EMUDA) is likely to prove particularly useful to chemists in their quest to study and model (potentially) auxetic structures such as the ones discussed here since chemists may be more familiar with molecular modelling techniques than with techniques relating to modelling of structures. We have shown that this EMUDA technique is particularly suitable for studying the properties of two-dimensional hexagonal honeycombs deforming though stretching or hinging of the rib elements, and in particular, it correctly predicts (within 11% accuracy) the magnitudes of the Poisson's ratios, including in cases when the systems exhibit auxetic behaviour [26].

This paper assesses the potential for auxetic behaviour of a novel class of structures which can be described as 'connected stars' as they contain star-shaped units which are connected together to form two-dimensional periodic structures. This study will be performed through the EMUDA technique as this offers the possibility

1
2
3
4
5
6
7
8
9
10
11
12
13
14
15
16
17
18
19
20
21
22
23
24
25
26
27
28
29
30
31
32
33
34
35
36
37
38
39
40
41
42
43
44
45
46
47
48
49
50
51
52
53
54
55
56
57
58
59
60

of analysing such systems very efficiently and relatively easily when compared to

more established (and laborious) methods of derivation of analytical equations (which

will not provide us with a tool for 'visualising' the deformation mechanisms) or

construction of real physical models (which cannot be easily modified so as to assess

the relative importance of the various structural properties).

2. The 'connected stars' structures

A macrostructure that has been extensively investigated for its auxetic properties is

the 'hexagonal re-entrant honeycomb' [27 - 29] deforming through hinging of the cell

walls which as illustrated in Fig. 1a, can be considered as a construct made from

'arrow-shaped building blocks'. However, the re-entrant hexagonal honeycomb is not

the only tessellate which can the constructed from 'arrows'. In fact, as illustrated in

Fig. 1, 'star-shaped building blocks' which have rotational symmetry of order $n = 3$, 4

and 6 (shown in bold in Fig. 1) may be built by connecting $n = 3$, 4 and 6 'arrows' in

such a way that the arms of the arrows form 'stars'. These building blocks can be used

to construct the periodic structures illustrated in Fig 1b-d, which shall henceforth be

referred to as STAR-3, STAR-4 and STAR-6 respectively, or collectively as STAR-n.

--- Insert Fig. 1 here ---

Given that these STAR-n structures contain the 'arrow-shaped' unit that is

responsible for the auxetic behaviour in idealised hinging re-entrant hexagonal

honeycomb, one may argue that these structures have a potential for exhibiting

auxetic behaviour, and in fact, the STAR-4 system (or constructs which are very similar to it) have been quoted as auxetic by several authors [30 - 32]. However, the STAR-3 and STAR-6 systems have not been invested as yet and no systematic investigation has been performed on the potential of these STAR-*n* structures as auxetics, possibly because of the increased complexity of the geometry when compared to the simpler re-entrant hexagonal honeycomb system.

In view of this, the EMUDA technique will be used to investigate these STAR-*n* systems (deforming though hinging at the vertices) in an attempt to obtain a better understanding of the potential of these systems as auxetics.

3. Modelling of the STAR-*n* systems

3.1 Description of the STAR-n systems through EMUDA

As illustrated in Fig. 2, the STAR-*n* systems can be constructed as periodic systems within a molecular modelling package using two types of dummy atoms, A and B. Under this description, the variables that need to be monitored during the simulation are:

   (i)   the bond lengths $|AB|$ and $|AA|$ where the length $|AB|$

            refers to the dimension of the stars whilst $|AA|$ refers to the

            length of the elements which connect the stars with each

            other;

   (ii)   the bond angles $A\hat{B}A$ and $A\hat{A}B$ where the angle $A\hat{B}A$

            refers to the acute angle in the stars whilst the angle $A\hat{A}B$

6

1
2
3
4
5
6
7
8
9
10
11
12
13
14
15
16
17
18
19
20
21
22
23
24
25
26
27
28
29
30
31
32
33
34
35
36
37
38
39
40
41
42
43
44
45
46
47
48
49
50
51
52
53
54
55
56
57
58
59
60

relate to the angles which are equivalent to the θ-hinges in the re-entrant honeycombs.

(iii)   the torsion angles ϕ_{AB} and ϕ_{AA} between four connected atoms A-A-B-A and B-A-A-B which must be set to $\pm 180^0$ and (0 *or* $\pm 180^0$) respectively (a requirement for constraining the systems system to remain planar).

--- Insert Figure 2 here ---

The energy expression would thus be of the form:

$$E = \sum_{\substack{\text{all AB} \\ \text{bonds}}} \frac{1}{2}k_s \left(|AB| - |AB|_0\right)^2 + \sum_{\substack{\text{all AA} \\ \text{bonds}}} \frac{1}{2}k_s \left(|AA| - |AA|_0\right)^2$$

$$+ \sum_{\substack{\text{all AAB} \\ \text{bond angles}}} \frac{1}{2}k_h^A \left(\left|A\hat{A}B\right| - \left|A\hat{A}B\right|_0\right)^2 + \sum_{\substack{\text{all ABB} \\ \text{bond angles}}} \frac{1}{2}k_h^B \left(\left|A\hat{B}B\right| - \left|A\hat{B}B\right|_0\right)^2$$

$$+ \sum_{\substack{\text{all A-A-B-A} \\ \text{torsion angles}}} \frac{1}{2}k_t \left[1 + \cos\left(\phi_{AB}\right)\right] + \sum_{\substack{\text{all B-A-A-B} \\ \text{torsion angles}}} \frac{1}{2}k_t \left[1 - \cos\left(2\phi_{AA}\right)\right]$$

where:

- $|AB|_0$, $|AA|_0$, $\left|A\hat{A}B\right|_0$ and $\left|A\hat{B}A\right|_0$ represent the values of the geometric parameters $|AB|$, $|AA|$, $\left|A\hat{A}B\right|$ and $\left|A\hat{B}A\right|$ respectively for the unloaded structures, where for the STAR-n structures to exhibit rotational symmetry of order n, the angles $\left|A\hat{A}B\right|_0$ and $\left|A\hat{B}A\right|_0$ must fulfil the condition imposed by Euclidean geometry on the sum of interior angles of a polygon that $n\left|A\hat{B}A\right|_0 + n\left(360^0 - \left|A\hat{A}B\right|_0\right) = \left(2n - 4\right)90^0$;

- k_s and k_t are the spring constants which define the resistance to 'stretching' (i.e. changes in bond lengths) and 'going out of plane' respectively, where in this case, since the structures are meant to remain planar and not deform through stretching, the force constants k_s and k_t must be set as high as possible;

- k_h^{A} and k_h^{B} are the 'hinging spring constants' where k_h^{A} defines the resistance to 'hinging of the $\left| \mathrm{A\hat{A}B} \right|$ angles' whilst k_h^{B} defines the resistance to 'hinging of the $\left| \mathrm{A\hat{B}A} \right|$ angles'. Note that these hinging force constants do not necessarily have the same values, but if the structures have to deform through hinging, these force constants must be smaller than k_s and k_t.

3.2 Simulation of the mechanical properties

The methodology used for the EMUDA simulations of the STAR-n was based on the methodology used by Grima *et al.* [26] for EMUDA modelling of hexagonal honeycombs and were performed using the molecular modelling package *Cerius^2* V3.0.

In particular, the systems were constructed using dummy atoms 'A' and 'B' using 3D periodic boundary conditions and aligned in the *YZ*-plane (which contains the (100) plane of the unit cell) as illustrated in fig. 2. This results in an infinite number of tessellates down the *X*-direction, which during the simulation were kept aligned with each other at a separation of 1Å from each other by constraining the unit

cell parameters a, β and γ to remain fixed during the simulation at 1Å, 90^0 and 90^0 respectively whilst leaving the unit cell parameters b, c and α as variables.

Custom-made force-fields were constructed with the parameters $\left|AB\right|_0$, $\left|AA\right|_0$, $\left|A\hat{A}B\right|_0$, $\left|A\hat{B}A\right|_0$, k_h^A and k_h^B set as described in Table 1, i.e. for each of the three different STAR-n structures, one set of parameters was chosen for the geometric variables $\left|AB\right|_0$, $\left|AA\right|_0$, $\left|A\hat{A}B\right|_0$ and $\left|A\hat{B}A\right|_0$ whilst twenty-five different combinations were used for the two hinging force-constant (the combinations allowed from $k_h^A, k_h^B \in \left\{ 50, 100, 200, 400, 800 \text{ kcal mol}^{-1} \text{ rad}^{-2} \right\}$).

--- Insert Table 1 here ---

The numerical values of the on-axis mechanical properties were calculated from the second derivative of the minimised energy expression whilst the off-axis Poisson's ratios were calculated by transforming the 3x3 compliance sub-matrix relating to the *YZ*-plane.

In particular, for systems (such as the ones discussed here) where the on-axis loading does not produce a shear strain, i.e.:

$$
\begin{pmatrix} \varepsilon_y \\ \varepsilon_z \\ \gamma_{yz} \end{pmatrix} = \begin{pmatrix} s_{22} & s_{23} & 0 \\ s_{32} & s_{33} & 0 \\ 0 & 0 & s_{44} \end{pmatrix} \begin{pmatrix} \sigma_y \\ \sigma_z \\ \tau_{yz} \end{pmatrix}
$$

the on-axis Poisson's ratios and Young's moduli are given by:

$$
E_y = \frac{\sigma_y}{\varepsilon_y} = \frac{1}{s_{22}} \qquad\qquad E_z = \frac{\sigma_z}{\varepsilon_z} = \frac{1}{s_{33}}
$$

$$\nu_{yz} = -\frac{\varepsilon_z}{\varepsilon_y} = -\frac{s_{32}}{s_{22}} \qquad\qquad \nu_{zy} = -\frac{\varepsilon_y}{\varepsilon_z} = -\frac{s_{23}}{s_{33}}$$

whilst the off-axis Poisson's ratios ν_{yz} after axis rotation by an angle ζ about the third

direction is given by:

$$\nu_{yz}(\zeta) = -\frac{m^4 s_{32} + m^2 n^2 (s_{22} + s_{33} - s_{44}) + n^4 s_{23}}{m^4 s_{22} + m^2 n^2 (s_{23} + s_{32} + s_{44}) + n^4 s_{33}}$$

where $m = \cos(\zeta)$ and $n = \sin(\zeta)$.

3.3 Results

Tables 2 - 3 show the on-axis Poison's ratios and Young's moduli of the STAR-n

systems having different values of k_h^A and k_h^B whilst Fig. 3 show the in-plane off-axis

Poisson's ratios of a selection of these system ($k_h^A, k_h^B \in \{50,800 \text{ kcal mol}^{-1} \text{ rad}^{-2}\}$).

--- Insert Table 2 here ---

--- Insert Table 3 here ---

--- Insert Fig. 3 here ---

These tables and figures clearly show that the three STAR-*n* systems have a

potential for exhibiting auxetic behaviour. In fact, the values of the on-axis Poisson's

ratios (Table 2) suggest that the three systems can exhibit negative Poisson's ratios for

some (but not all) values of k_h^A and k_h^B. Furthermore, since all Young's moduli are

less than 10,000GPa, the simulated properties of the STAR-*n* systems are likely to be

within ±10% of the actual values [26].

Table 2 also suggests that the STAR-4 and STAR-6 systems have a greater

potential for exhibiting auxetic behaviour than the STAR-3 systems as these can

achieve negative on-axis Poisson's ratios for a much larger range of force-constants.

In this respect, the STAR-4 systems appear to be superior to the STAR-6 systems as

these can exhibit lower (i.e. more negative) values of the on-axis Poisson's ratios.

However, the off-axis Poisson's ratio highlight an important difference in the

properties of these systems, namely that whilst the Poisson's ratios for the STAR-3

and STAR-6 systems are independent on the direction of loading (a result of the

symmetry of these systems), the STAR-4 systems are anisotropic and the magnitudes

of the Poisson's ratio are dependent on the direction of loading. In these systems,

maximum auxeticity is exhibited for loading parallel to the major axis whilst

conventional behaviour is exhibited for loading at 45^0 to the major axis, thus making

the STAR-6 systems 'more auxetic'.

4. Explaining the measured Poisson's ratios in terms of the deformation mechanisms

The presence or otherwise of auxetic behaviour, and the particular values of

the Poisson's ratios in the STAR-n systems may be explained by looking at the

deformations that result from uniaxial loading of these systems. It should be noted

that this analysis is not trivial as the conditions required for the STAR-n systems to

exhibit auxetic behaviour are different for systems with different symmetry, and

hence each of the three STAR-n systems must be considered independently.

--- Insert Fig. 4 here ---

--- Insert Fig. 5 here ---

--- Insert Fig. 6 here ---

In view of this we have performed simulations where a selection of the STAR-
n systems were loaded in the Z-direction with loads within the range of $\pm 0.1E_z$. The
shapes of resulting 'loaded' structures were then compared (see Fig. 4 - 6) and the
variation of various angles were monitored in an attempt to obtain a better
understanding of the way that the various geometric parameters of the different
systems change as a result of the applied loads (see Fig. 7 - 9).

--- Insert Fig. 7 here ---

--- Insert Fig. 8 here ---

--- Insert Fig. 9 here ---

4.1 The STAR-3 systems

The results in Table 2a suggest that in the case of the STAR-3 systems,
auxeticity is only exhibited in situations when the force-constant k_h^A is much higher
than k_h^B. As illustrated in Fig. 1, the geometry of the STAR-3 systems may be
described as a regular 'hexagonal honeycomb' with 'three-pointed stars' located at its
vertices. In such systems, the values of the Poisson's ratios depend on the relative
extent of deformations of these two structural components, i.e. the 'honeycomb' and
the 'stars'. (Deformations where the 'stars' open up when the system is stretched
result in auxetic behaviour whilst deformations of the 'hexagonal honeycomb' result

in conventional behaviour.) This is illustrated very clearly in the simulations (see Fig. 4 and Fig. 7) which show that:

(a) When $k_h^B >> k_h^A$, the stars can be treated as rigid units and uniaxial loading will primarily result in a deformation of the hexagonal honeycomb which makes the system exhibit a high positive Poisson's ratio. In fact, the STAR-3 structure with $k_h^A =$ 50 kcal mol^{-1} rad^{-2} and $k_h^B =$ 800 kcal mol^{-1} rad^{-2} deforms in a such a way that as illustrated in Fig 4b and Fig. 7b, the angle θ changes at a much higher rate than β_1 and β_2 with the result that the system exhibits Poison's a ratio of +0.873.

(b) As k_h^B decreases with k_h^A remaining low, the stars start to loose their rigidity open up with the result that deformations of the 'stars' will start to occur concurrently with the deformations of the 'hexagonal honeycomb'. A similar net result can be achieved if the value of k_h^A is increased whilst k_h^B remains high, as this would restrict deformations of the 'hexagonal honeycomb' with the result that the two types of deformations will be permitted to occur concurrently. These changes will result in a lowering of the Poisson's ratios, an effect which is seen very clearly in the STAR-3 systems with $k_h^A = k_h^B =$ 50 kcal mol^{-1} rad^{-2} and $k_h^A = k_h^B =$ 800 kcal mol^{-1} rad^{-2} which exhibit Poisson's ratios of +0.292 and +0.247 respectively (compared to +0.873 for the system with $k_h^A =$ 50 kcal mol^{-1} rad^{-2} and $k_h^B =$ 800 kcal mol^{-1} rad^{-2}). It should be also

noted that the system with $k_h^A = k_h^B = 800$ kcal mol^{-1} rad^{-2} will be

much stiffer than the system with $k_h^A = k_h^B = 50$ kcal mol^{-1} rad^{-2}

(see Table 3a for a comparison of the moduli).

(c)   Auxetic behaviour can be obtained if $k_h^A >> k_h^B$. These systems,

such as the one with $k_h^A = 800$ kcal mol^{-1} rad^{-2} and $k_h^B = 50$ kcal

mol^{-1} rad^{-2}, are characterised by having a high Young's modulus

(see Table 3a) since a high k_h^A will restrict deformations of the

BAB angles which will in turn restrict changes in the shape of the

stars. However, the high values of the force-constants high k_h^A and

the small value of k_h^B will result in a situation where the

deformations of the 'stars' (i.e. changes in β_1 and β_2) will occur at

a higher rate than deformations of the 'hexagonal honeycomb' (i.e.

changes in θ, see Fig 4c and Fig. 7c) with the net result that the

system can exhibit negative Poisson's ratios ($\nu_{zy} = -0.163$).

4.2 The STAR-4 systems

The results in Table 2b suggest that in the case of the STAR-4 systems,

auxeticity is exhibited for most combinations of the force-constants, but for low

values of k_h^A, the auxeticity decreases as k_h^B increases, to the extent that the STAR-4

system with $k_h^A = 50$ kcal mol^{-1} rad^{-2} and $k_h^B = 800$ kcal mol^{-1} rad^{-2} exhibits

conventional behaviour. In these systems, a combination of force-constants where k_h^B

14

$\gg k_h^A$ results in a situation where the 'ABA triangles' in the stars assume a rigid

shape (the β angles in Fig. 8e remain constant) with the consequence that when loads

are applied, these triangles rotate relative to each other (due to changes in the α

angles) with the net effect that as illustrated in Fig. 10, the main deformation is one

involving changes in the shape of the 'AAAA quadrilateral' which opens / closes in a

'wine-rack' type fashion hence producing the observed positive Poisson's ratios. This

type of behaviour is observed in the system with $k_h^A = 50$ kcal mol^{-1} rad^{-2} and $k_h^B =$

800 kcal mol^{-1} rad^{-2} where as illustrated in Fig. 8b, uniaxial loading results primarily

in changes in the α angles whilst the β angles remain constant. For other

combinations of the force-constants, the auxetic effect in the STAR-4 systems is due

to deformations which involve 'opening up of the stars' where as illustrated in Fig.

8a,c & d, uniaxial loading results in changes in the α and β angles which increase in

magnitude when the system is loaded.

--- Insert Fig. 10 here ---

4.3 The STAR-6 systems

The STAR-6 systems behave very similarly to the STAR-4 system and once again,

auxetic behaviour is exhibited for most combinations of the force-constants. However,

for these systems, the auxetic effect decreases under two conditions:

    (i)   for low values of k_h^A, the auxeticity decreases as k_h^B

                 increases, to the extent that the STAR-6 system with $k_h^A =$

50 kcal mol^{-1} rad^{-2} and $k_h^B = 800$ kcal mol^{-1} rad^{-2} exhibits

conventional behaviour;

(ii)   for low values of k_h^B, the auxeticity decreases as k_h^A

increases, to the extent that the STAR-6 system with $k_h^B =$

50 kcal mol^{-1} rad^{-2} and $k_h^A = 800$ kcal mol^{-1} rad^{-2} exhibits

conventional behaviour.

The conventional behaviour of STAR-6 systems with $k_h^B >> k_h^A$ can be explained in a

similar way to that of the analogous STAR-4 systems since, as illustrated in Fig. 11a,

these systems behave in such a way where the 'ABA triangles' in the stars assume a

rigid shape (the β angles in Fig. 9e remain constant) with the consequence that when

loads are applied, some of these triangles rotate relative to each other (due to changes

in the α angles) with the net effect that as illustrated in Fig. 11a, the main deformation

is one involving changes in the shape of the 'AAAAAA hexagon' which generates

positive Poisson's ratios. Furthermore, as illustrated in Fig. 11b, the behaviour of

systems where $k_h^B << k_h^A$ can also be explained using similar arguments since in

such systems, the high value of k_h^A forces the 'BAB triangles' in the stars assume a

rigid shape (the α angles in Fig. 9e remain constant) with the consequence that when

loads are applied, the changes in the β angles result in the net effect that as illustrated

in Fig. 11b, the main deformation is one involving changes in the shape of the

'BBBBBB hexagon' which generates positive Poisson's ratios.

--- **Insert Fig. 11 here** ---

16

1
2
3
4
5
6
7
8
9
10
11
12
13
14
15
16
17
18
19
20
21
22
23
24
25
26
27
28
29
30
31
32
33
34
35
36
37
38
39
40
41
42
43
44
45
46
47
48
49
50
51
52
53
54
55
56
57
58
59
60

5. Conclusions

This work has examined through the EMUDA technique (a method of analysis based on force-field molecular modelling simulations) the potential as auxetics of a novel class of two dimensional periodic structures which can be described as 'connected stars' where the stars have rotational symmetry of order 3, 4 or 6.

This work is highly significant on two accounts: First, it has shown that these 'star' containing systems have a potential for auxetic behaviour. In particular, it has been shown that the systems made from stars of rotational symmetry of order 6 and 4 have a greater potential for exhibiting auxetic behaviour than the systems with rotational symmetry of order 3. We have also shown that the magnitudes of the Poisson's ratios are effected by the stiffness of the hinges which connect the different rod elements of the structure, and that the different systems are effected differently if the stiffness of the hinges are altered.

Secondly, this work has also shown the ease by which the EMUDA technique can be implemented to study the behaviour of periodic strictures under applied loads, and in particular to examine whether such systems are auxetic or not. In particular, we have been able to assess which systems are most promising as auxetics without the need of constructing real physical models or deriving analytical equations, hence accelerating the analysis of these systems, as the most promising systems can be given priority over the others in a more in-dept study, where, for example, the geometric parameters will also be set as variables.

References:

1   K.E. Evans, M.A. Nkansah, I.J. Hutchinson, S.C. Rogers. Molecular network
    design. *Nature*, **353**, 124 (1991).

2   R. Lakes. Foam structures with a negative Poisson's ratio. *Science*, **235**, 1038
    (1987).

3   R.S. Lakes, K. Elms. Indentability of conventional and negative Poisson's ratio
    foams. *J. Compos. Mater.*, **27**, 1193 (1993).

4   J. B. Choi, R. S. Lakes. Analysis of elastic modulus of conventional foams and of
    reentrant foam materials with a negative Poisson's ratio. *Int. J. Mech. Sci.*, **37**, 51
    (1995).

5   N. Chan, K. E. Evans. Microscopic examination of the microstructure and
    deformation of conventional and auxetic foams. *J. Mater. Sci.*, **32**, 5725 (1997).

6   C.W. Smith, J.N. Grima, K.E. Evans. A novel mechanism for generating auxetic
    behaviour in reticulated foams: Missing rib foam model. *Acta Materiala*, **48**, 4349
    (2000).

7   J. N. Grima, A. Alderson, K. E. Evans. An alternative explanation for the negative
    Poisson's ratio in auxetic foams. *J. Phys. Soc. Jpn.*, **74**, 1341 (2005).

8   R.H. Baughman, D.S. Galvao. Crystalline networks with unusual predicted
    mechanical and thermal-properties. *Nature*, **365**, 735 (1993).

9   J.N. Grima, K.E. Evans. Self expanding molecular networks. *Chem. Comm.*, **16**,
    1531 (2000).

10 J.N. Grima, J.J. Williams, K.E. Evans. Networked calix[4]arene polymers with
    unusual mechanical properties. *Chem. Comm.*, **32**, 4065, (2005)

18

11 C.B. He, P.W. Liu, A. C. Griffin. Toward negative Poisson ratio polymers through molecular design. *Macromolecules*, **31**, 3145 (1998).

12 C.B. He, P.W. Liu, P.J. McMullan, A.C. Griffin. Toward molecular auxetics: Main chain liquid crystalline polymers consisting of laterally attached para-quaterphenyls. *Phys. Stat. Sol. (b)*, **242** 576 (2005).

13 K.E. Evans, B.D. Caddock. Microporous materials with negative poisson ratios .2. Mechanisms and interpretation. *J. Phys. D: Appl. Phys*., **22**, 1877 (1989).

14 K.L. Alderson, K.E. Evans. Strain-dependent behavior of microporous polyethylene with a negative Poisson ratio. *J. Mater. Sci*. **28**, 4092 (1993).

15 A.P. Pickles, K.L. Alderson, K.E. Evans. The effects of powder morphology on the processing of auxetic polypropylene (PP of negative Poisson's ratio). *Polym. Eng. & Sci.*, **36**, 636 (1996).

16 R.H. Baughman, J.M. Shacklette, A.A. Zakhidov, S. Stafstrom. Negative Poisson's ratios as a common feature of cubic metals. *Nature*, **392**, 362 (1998).

17 N. R. Keskar, J. R. Chelikowsky. Negative Poisson ratios in crystalline SiO_2 from 1st-principles calculations. *Nature*, **358**, 222 (1992).

18 A. Yeganeh-Haeri, D. J. Weidner, J. B. Parise. Elasticity of alpha-cristobalite - a silicon dioxide with a negative Poisson's ratio. *Science*, **257,** 650 (1992).

19 A. Alderson, K. E. Evans. Rotation and dilation deformation mechanisms for auxetic behaviour in the alpha-cristobalite tetrahedral framework structure. *Phys. Chem. Miner.*, **28**, 711 (2001).

20 A. Alderson, K.L. Alderson, K.E. Evans, J.N. Grima, M. Williams. Modelling of Negative Poisson's Ratio Nanomaterials: Deformation Mechanisms, Structure-Property Relationships and Applications. *J. Metastable Nanocryst. Mater.*, **23**, 55, (2005).

21 A. Alderson, K.L. Alderson, K.E. Evans, J.N. Grima, M.R. Willams, P.J. Davies. Modelling the deformation mechanisms, structure-property relationships and applications of auxetic nanomaterials. *Phys. Status Solidi B*, **242**, 499 (2005).

22 J.N. Grima, R. Gatt, A. Alderson, K.E. Evans. On the origin of auxetic behaviour in the silicate α-cristobalite. *J. Mater. Chem.*, DOI: 10.1039/b508098c (2005).

23 J.N. Grima, R. Jackson, A. Alderson, K.E. Evans. "Do zeolites have negative Poisson's ratios?" *Advanced Materials*, **12**, 1912 (2000).

24 A. Alderson. A triumph of lateral thought. *Chem. Ind.*, **10**, 384 (1999).

25 J. N. Grima, K. E. Evans. Auxetic behaviour from rotating squares. *J. Mater. Sci. Lett.*, **19**, 1563 (2000).

26 J.N. Grima, R. Gatt, T. G. Chircop-Bray, A. Alderson, K.E. Evans. Empirical Modelling Using Dummy Atoms (EMUDA): An alternative approach for studying 'auxetic' structures. Submitted to *Molecular Simulations* (2005).

27 F.K. Abd el-Sayed, R. Jones, I.W. Burgens. Theoretical approach to the deformation of honeycomb based composite-materials. *Composites*, **10**, 209 (1979).

28 L.J. Gibson, M.F. Ashby. Cellular Solids: Structure and Properties, Oxford: Pergamon, Oxford (1988).

29 I.G. Masters, K.E. Evans. Models for the elastic deformation of honeycombs. *Compos. Struct.*, **35**, 403 (1996).

30 F.R. Attenborough. The modelling of network polymers. Ph.D. Thesis, University of Liverpool, UK (1997).

31 W. Yang, Z.M. Li, B.H. Xie, W. Shi, M.B. Yang. On Auxetic materials. *J. Mater. Sci.*, **39**, 3269 (2004).

32 P.S. Theocaris, G.E. Stavroulakis, P.D. Panagiotopoulos. Negative Poisson's

    ratios in composites with star-shaped inclusion: A numerical homogenisation

    approach. *Arch. Appl. Mech.*, **67**, 274 (1997).

Acknowledgements

Tables:

Table 1

Parameters in Eqn. 5:	Values used:
$\left\vert AB\right\vert_0$, $\left\vert AA\right\vert_0$	1Å, 2Å
$\left\vert A\hat{A}B\right\vert_0$, $\left\vert A\hat{B}A\right\vert_0$	70^0, 20^0 for STAR-3 55^0, 20^0 for STAR-4 40^0, 20^0 for STAR-6
(k_h^A , k_h^B)	$k_h^A, k_h^B \in \left\{50, 100, 200, 400, 800 \text{ kcal mol}^{-1} \text{ rad}^{-2}\right\}$ i.e. (k_h^A , k_h^B) = (50, 50); (50, 100); (50, 200); (50, 400); … (800, 400); (800, 800) kcal mol^{-1} rad^{-2}

Table 1: Parameters used for the custom-made force-fields

Table 2

k_h^A \ k_h^B		50	100	200	400	800
50	ν_{yz}	0.292	0.484	0.667	0.793	0.872
	ν_{zy}	0.292	0.496	0.667	0.793	0.873
100	ν_{yz}	0.103	0.288	0.486	0.658	0.782
	ν_{zy}	0.103	0.287	0.486	0.658	0.782
200	ν_{yz}	-0.036	0.100	0.281	0.475	0.642
	ν_{zy}	-0.036	0.100	0.281	0.475	0.642
400	ν_{yz}	-0.121	-0.036	0.096	0.269	0.453
	ν_{zy}	-0.121	-0.036	0.096	0.269	0.453
800	ν_{yz}	-0.163	-0.116	-0.036	0.087	0.247
	ν_{zy}	-0.163	-0.116	-0.036	0.087	0.247

Table 2a: The on-axis Poisson's ratios for the STAR-3 systems for various combinations of the force-constants k_h (in kcal mol^{-1} rad^{-2}).

k_h^A \ k_h^B		50	100	200	400	800
50	ν_{yz}	-0.794	-0.690	-0.476	-0.228	0.079
	ν_{zy}	-0.794	-0.678	-0.530	-0.228	0.079
100	ν_{yz}	-0.835	-0.760	-0.633	-0.432	-0.163
	ν_{zy}	-0.845	-0.760	-0.633	-0.432	-0.163
200	ν_{yz}	-0.834	-0.785	-0.697	-0.549	-0.331
	ν_{zy}	-0.834	-0.785	-0.697	-0.549	-0.331
400	ν_{yz}	-0.799	-0.765	-0.701	-0.590	-0.415
	ν_{zy}	-0.799	-0.765	-0.701	-0.590	-0.415
800	ν_{yz}	-0.719	-0.694	-0.647	-0.562	-0.424
	ν_{zy}	-0.719	-0.694	-0.647	-0.562	-0.425

Table 2b: The on-axis Poisson's ratios for the STAR-4 systems for various combinations of the force-constants k_h (in kcal mol^{-1} rad^{-2}).

k_h^{A} \\ k_h^{B}		50	100	200	400	800
50	ν_{yz}	-0.451	-0.418	-0.314	-0.078	0.132
	ν_{zy}	-0.451	-0.413	-0.315	-0.070	0.132
100	ν_{yz}	-0.406	-0.435	-0.396	-0.274	-0.071
	ν_{zy}	-0.398	-0.434	-0.396	-0.274	-0.071
200	ν_{yz}	-0.265	-0.375	-0.403	-0.347	-0.204
	ν_{zy}	-0.265	-0.375	-0.404	-0.347	-0.204
400	ν_{yz}	-0.082	-0.248	-0.342	-0.349	-0.264
	ν_{zy}	-0.082	-0.249	-0.343	-0.349	-0.264
800	ν_{yz}	0.126	-0.126	-0.219	-0.288	-0.262
	ν_{zy}	0.129	-0.139	-0.220	-0.288	-0.262

Table 2c: The on-axis Poisson's ratios for the STAR-6 systems for various combinations of the force-constants k_h (in kcal mol^{-1} rad^{-2}).

Table 3

k_h^A \ k_h^B		50	100	200	400	800
50	E_y	327.289	376.889	449.014	512.033	574.482
	E_z	327.011	386.145	449.014	512.059	574.911
100	E_y	547.885	649.393	766.636	889.917	1013.120
	E_z	548.637	648.256	766.636	889.917	1013.140
200	E_y	941.265	1081.853	1277.368	1508.000	1748.038
	E_z	941.176	1081.853	1277.286	1508.318	1748.282
400	E_y	1669.728	1839.148	2108.192	2481.513	2922.012
	E_z	1669.505	1839.080	2108.192	2481.513	2922.182
800	E_y	3026.268	3204.512	3516.669	4012.680	4697.261
	E_z	3026.176	3204.512	3516.669	4012.519	4697.261

Table 3a: The on-axis Young's moduli for the STAR-3 systems for various

combinations of the force-constants k_h (in kcal mol^{-1} rad^{-2}).

k_h^B / k_h^A		50	100	200	400	800
50	E_y	955.840	1471.865	2335.957	3573.726	4994.756
	E_z	955.840	1446.278	2599.496	3573.854	4990.767
100	E_y	1234.035	1860.500	2846.003	4399.666	6480.881
	E_z	1248.439	1860.500	2846.003	4399.859	6481.722
200	E_y	1938.774	2503.317	3531.822	5262.050	7810.059
	E_z	1938.774	2503.317	3531.822	5262.327	7810.059
400	E_y	3136.566	3672.285	4670.496	6411.900	9135.757
	E_z	3136.566	3672.420	4670.496	6411.900	9141.603
800	E_y	5282.341	5753.740	6642.753	8233.163	10825.205
	E_z	5282.341	5753.740	6642.753	8233.841	10827.198

Table 3b: The on-axis Young's moduli for the STAR-4 systems for various combinations of the force-constants k_h (in kcal mol^{-1} rad^{-2}).

k_h^A \ k_h^B		50	100	200	400	800
50	E_y	672.133	1094.260	1811.233	2838.490	4241.062
	E_z	672.133	1082.263	1812.842	2537.878	4241.242
100	E_y	849.907	1322.891	2134.517	3466.565	5385.610
	E_z	834.168	1321.755	2136.113	3466.565	5385.900
200	E_y	1166.398	1686.426	2567.526	4060.419	6391.001
	E_z	1169.016	1686.284	2569.307	4065.041	6392.227
400	E_y	1653.057	2279.670	3241.176	4852.484	7415.097
	E_z	1656.068	2283.314	3255.314	4854.369	7416.197
800	E_y	2335.575	2819.284	4383.466	6109.109	8785.030
	E_z	2388.174	3116.236	4386.735	6110.975	8786.574

Table 3c: The on-axis Young's moduli for the STAR-6 systems for various combinations of the force-constants k_h (in kcal mol^{-1} rad^{-2}).

1
2
3
4
5
6
7
8
9
10
11
12
13
14
15
16
17
18
19
20
21
22
23
24
25
26
27
28
29
30
31
32
33
34
35
36
37
38
39
40
41
42
43
44
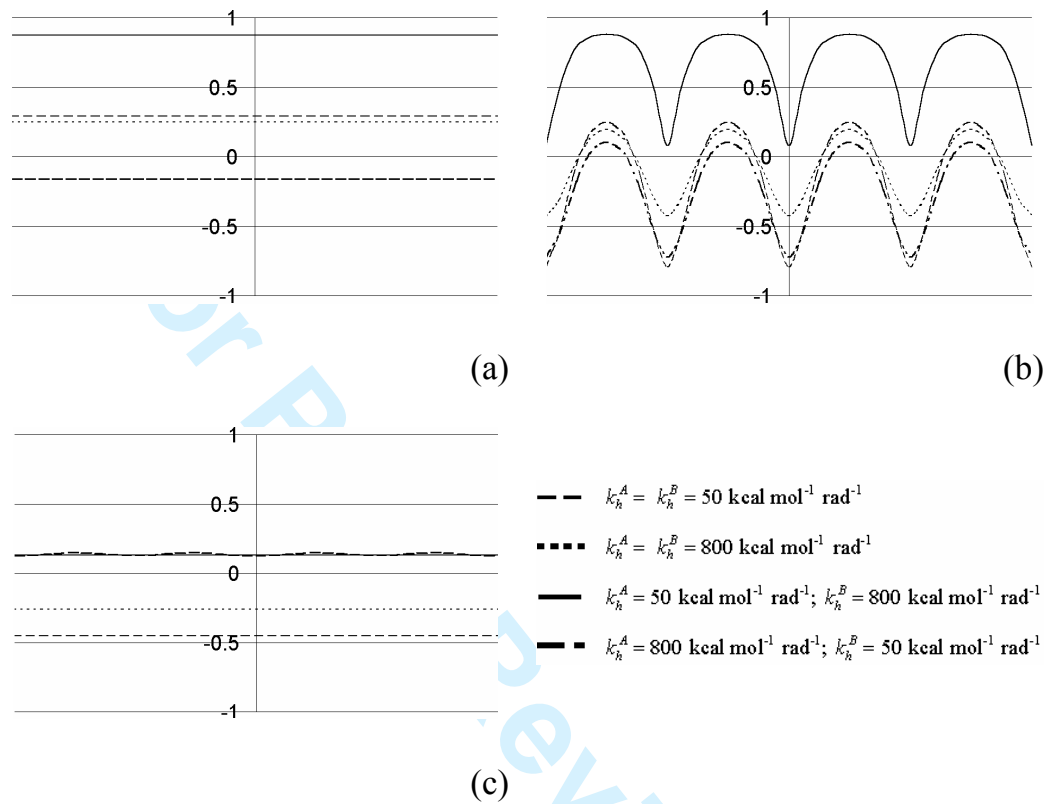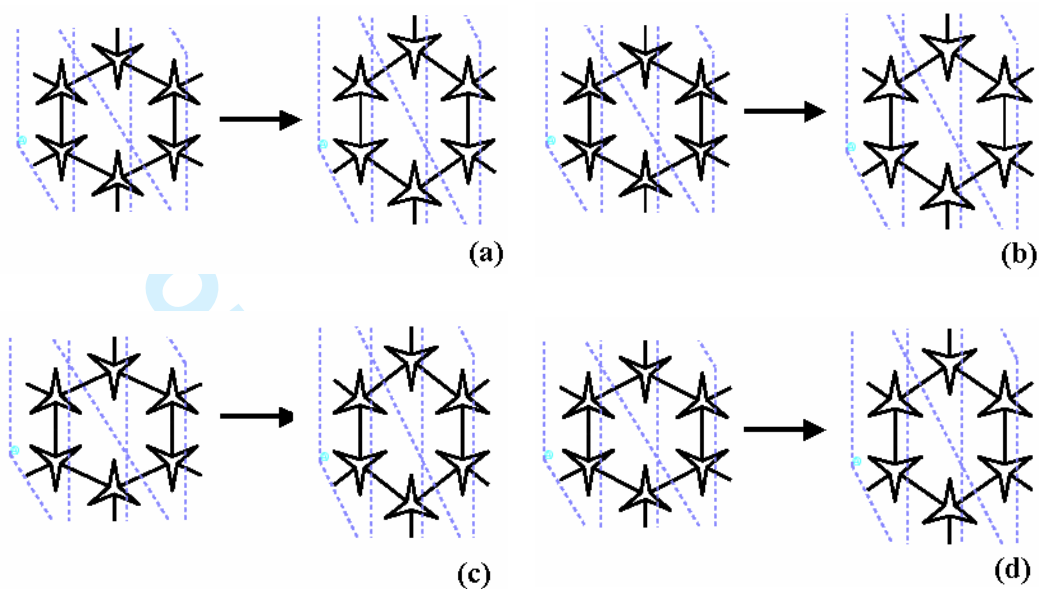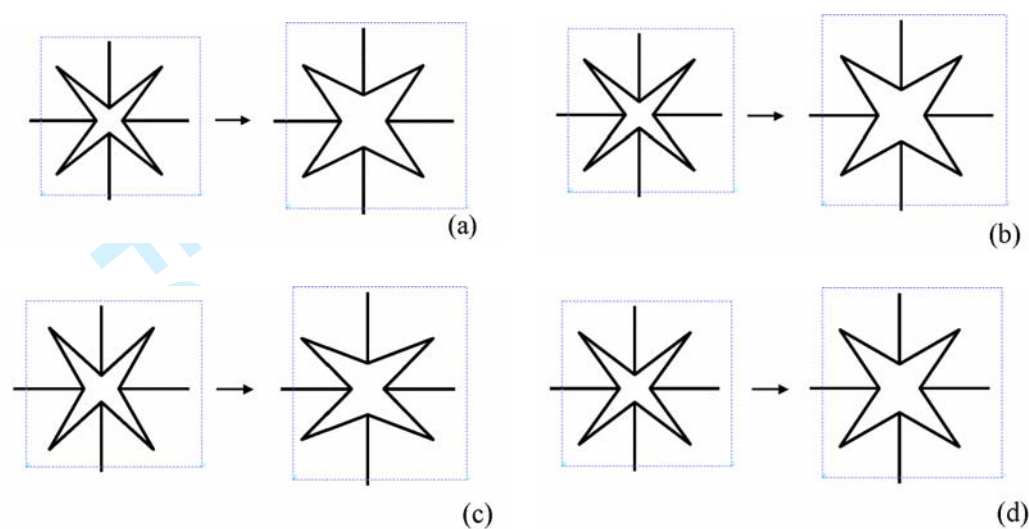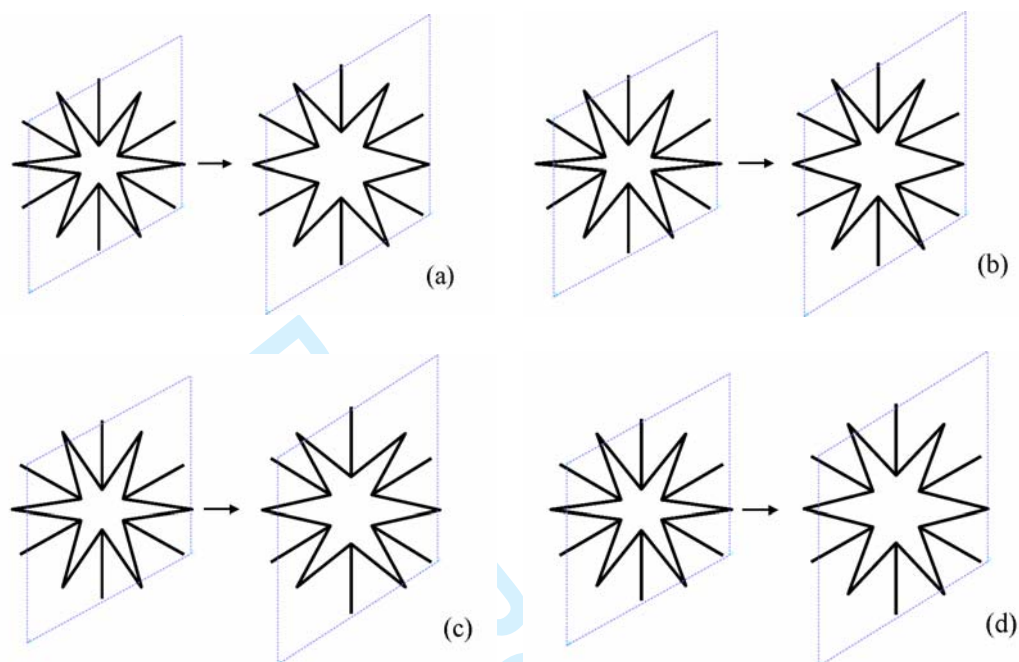45
46
47
48
49
50
51
52
53
54
55
56
57
58
59
60

Figures:

Figure 1

Figure 2

(a)

(b)

(c)

1
2
3
4
5
6
7
8
9
10
11
12
13
14
15
16
17
18
19
20
21
22
23
24
25
26
27
28
29
30
31
32
33
34
35
36
37
38
39
40
41
42
43
44
45
46
47
48
49
50
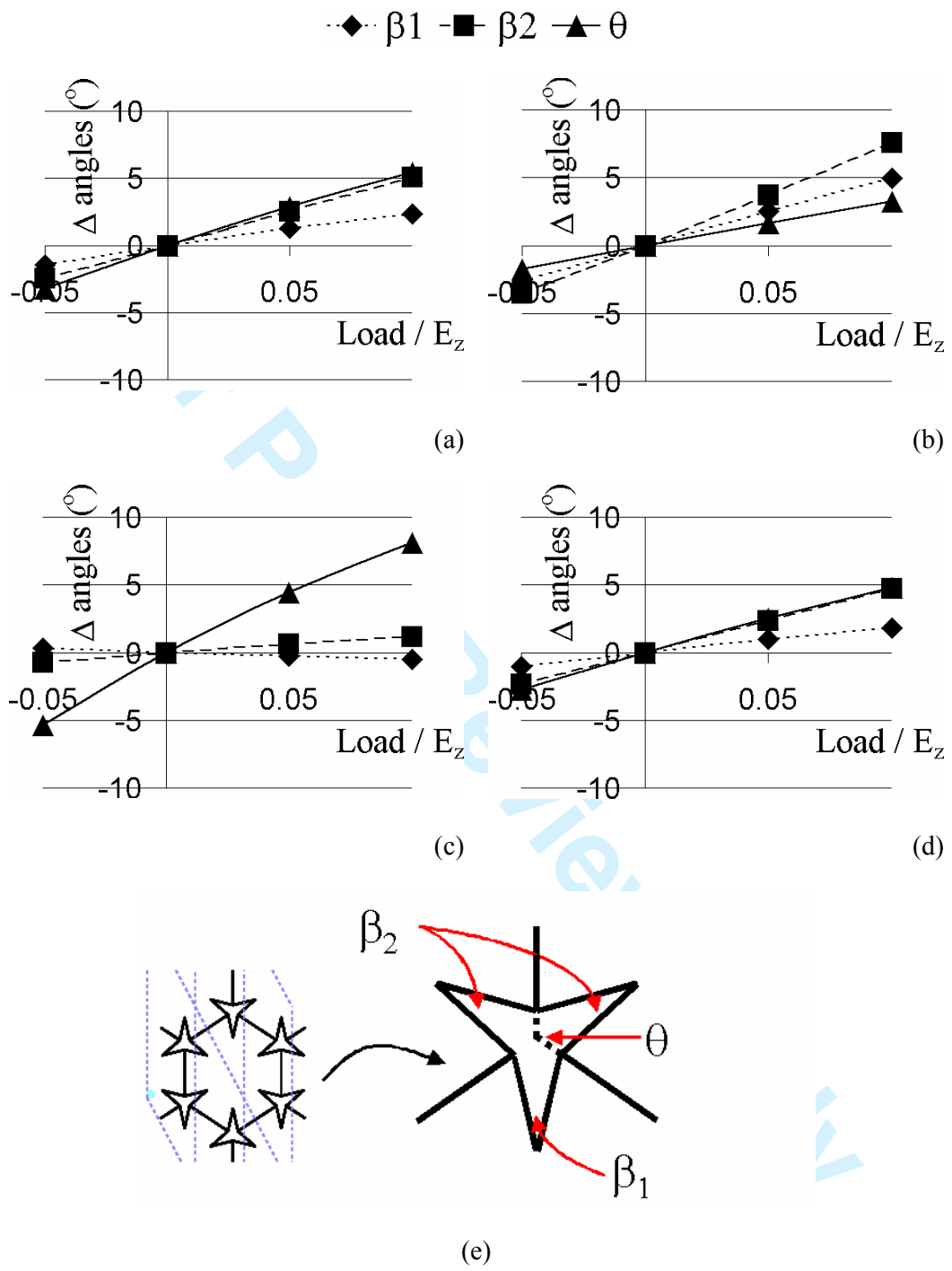51
52
53
54
55
56
57
58
59
60

Figure 3

(a)

(b)

(c)

$k_h^A = k_h^B = 50$ kcal mol^{-1} rad^{-1}

$k_h^A = k_h^B = 800$ kcal mol^{-1} rad^{-1}

$k_h^A = 50$ kcal mol^{-1} rad^{-1}; $k_h^B = 800$ kcal mol^{-1} rad^{-1}

$k_h^A = 800$ kcal mol^{-1} rad^{-1}; $k_h^B = 50$ kcal mol^{-1} rad^{-1}

Figure 4

(a)

(b)

(c)

(d)

32

1
2
3
4
5
6
7
8
9
10
11
12
13
14
15
16
17
18
19
20
21
22
23
24
25
26
27
28
29
30
31
32
33
34
35
36
37
38
39
40
41
42
43
44
45
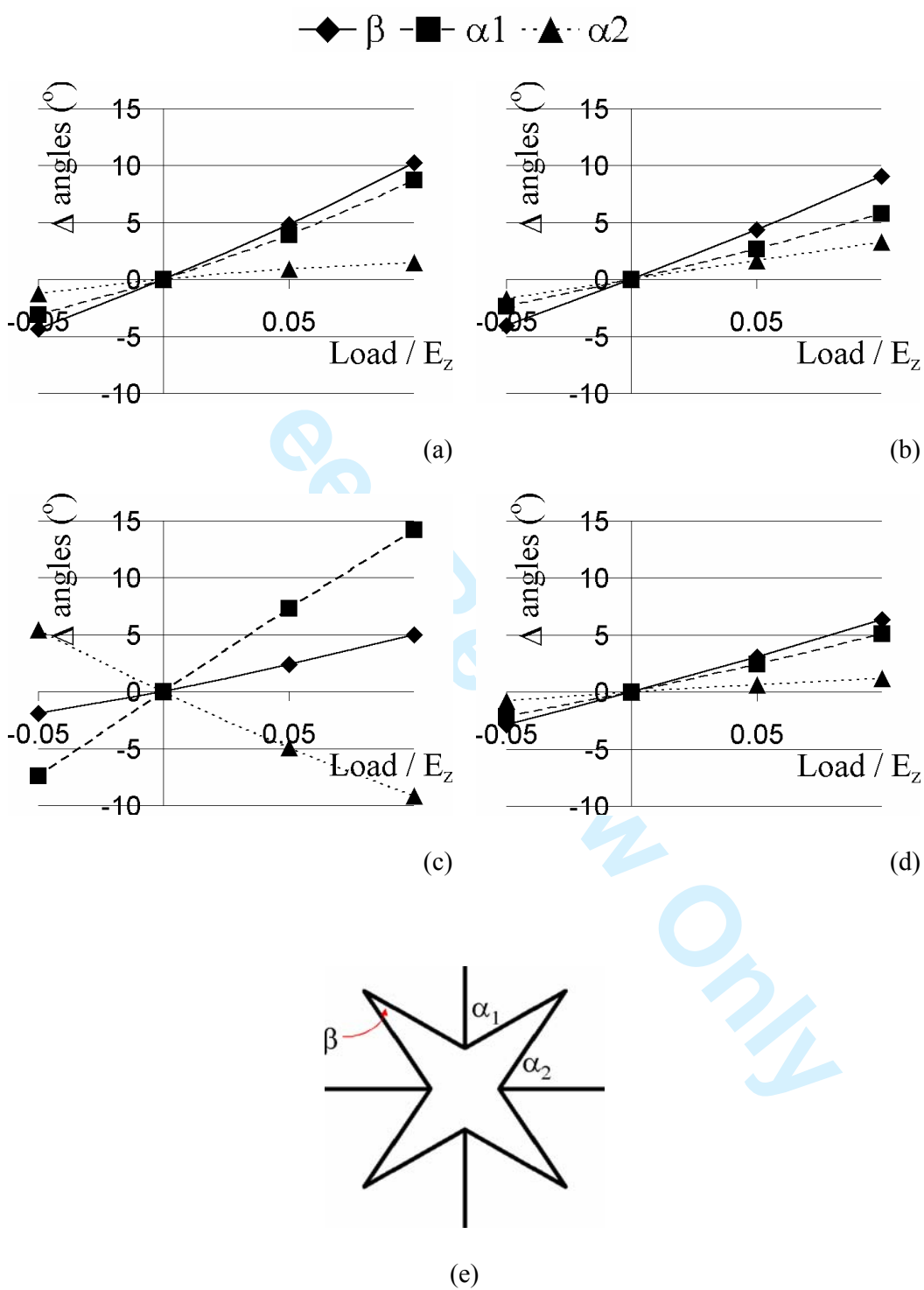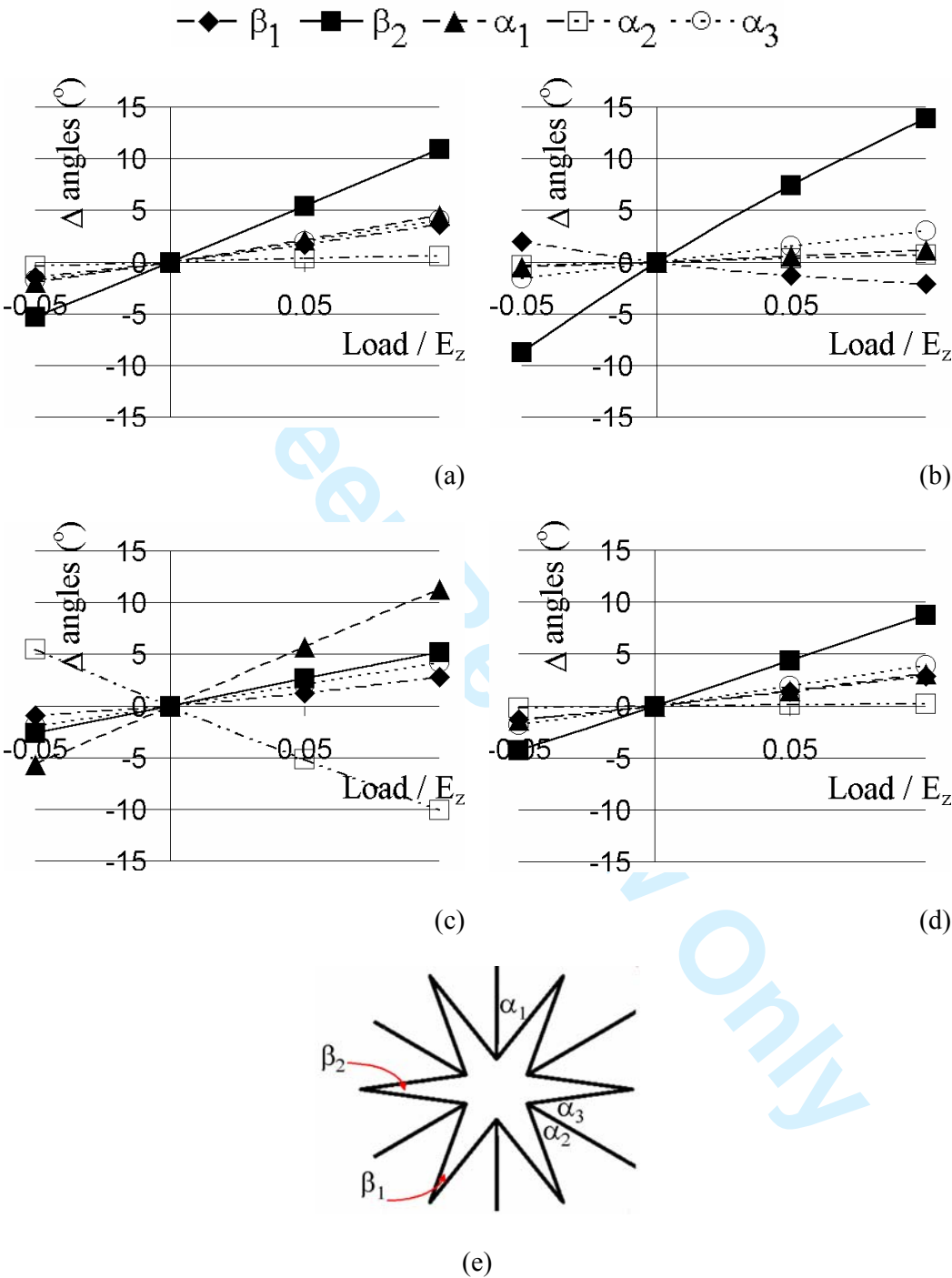46
47
48
49
50
51
52
53
54
55
56
57
58
59
60
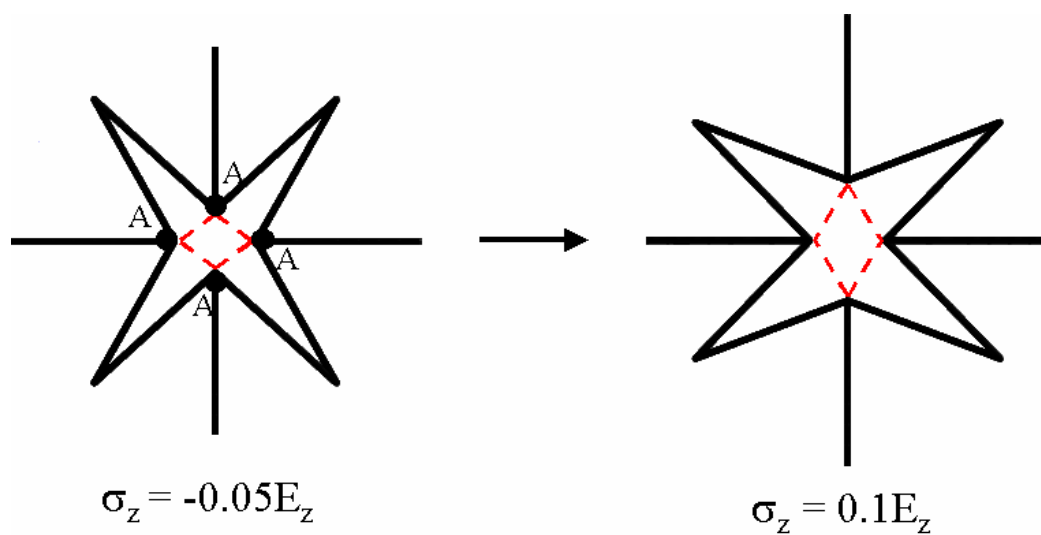
Figure 5

(a)

(b)

(c)

(d)

Figure 6

34

1
2
3
4
5
6
7
8
9
10
11
12
13
14
15
16
17
18
19
20
21
22
23
24
25
26
27
28
29
30
31
32
33
34
35
36
37
38
39
40
41
42
43
44
45
46
47
48
49
50
51
52
53
54
55
56
57
58
59
60

Figure 7
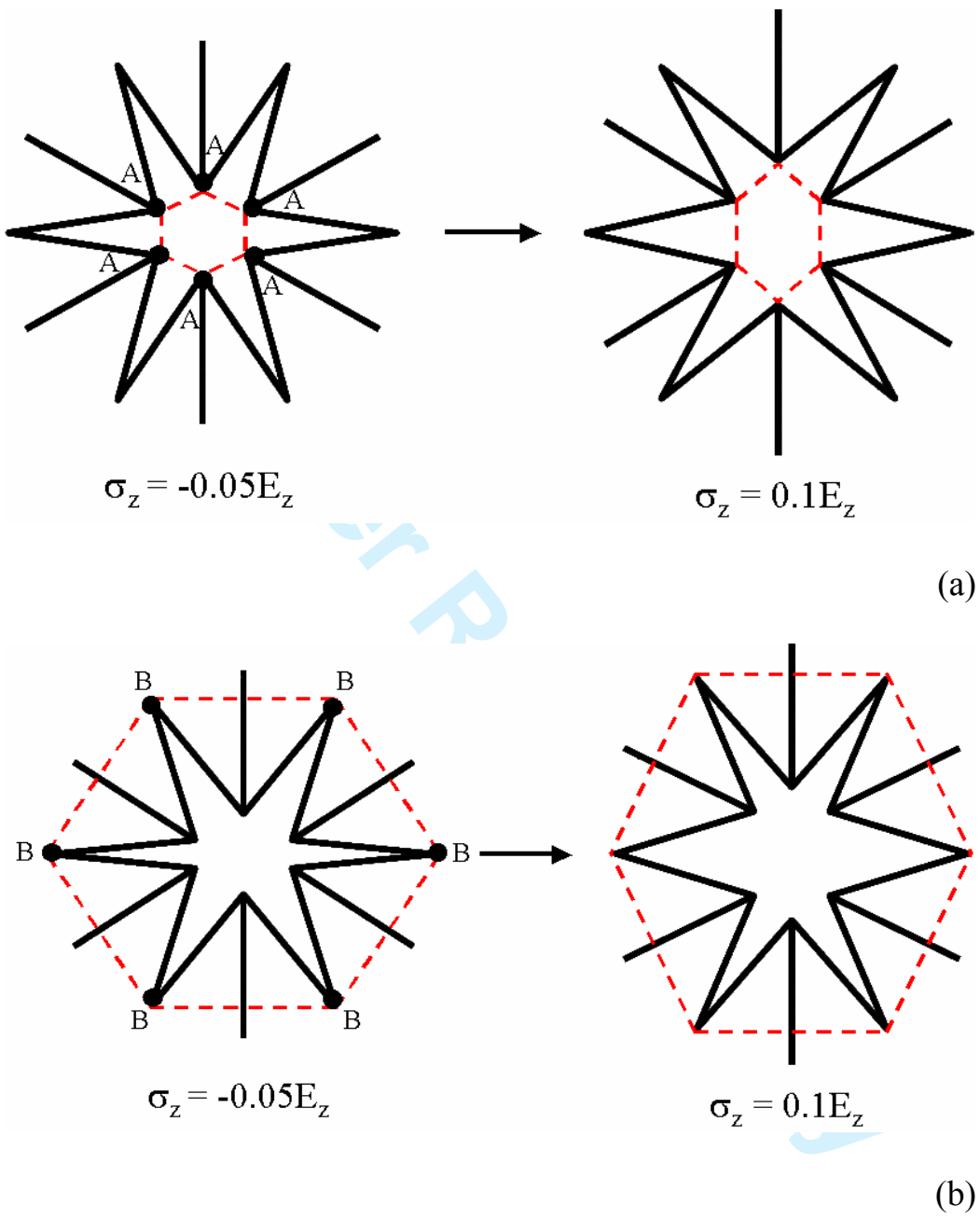

(a)

(b)

(c)

(d)

(e)

Figure 8

(a)

(b)

(c)

(d)

(e)

1
2
3
4
5
6
7
8
9
10
11
12
13
14
15
16
17
18
19
20
21
22
23
24
25
26
27
28
29
30
31
32
33
34
35
36
37
38
39
40
41
42
43
44
45
46
47
48
49
50
51
52
53
54
55
56
57
58
59
60

Figure 9

(a)

(b)

(c)

(d)

(e)

Figure 10

$$\sigma_z = -0.05E_z \qquad\qquad\qquad \sigma_z = 0.1E_z$$

38

1
2
3
4
5
6
7
8
9
10
11
12
13
14
15
16
17
18
19
20
21
22
23
24
25
26
27
28
29
30
31
32
33
34
35
36
37
38
39
40
41
42
43
44
45
46
47
48
49
50
51
52
53
54
55
56
57
58
59
60

Figure 11

$\sigma_z = -0.05E_z$ $\sigma_z = 0.1E_z$

(a)

$\sigma_z = -0.05E_z$ $\sigma_z = 0.1E_z$

(b)

Captions:

Figure 1: . Various tessellations which can the constructed from 'arrows'. When $n =$ 2, 3, 4, 6, an auxetic honeycomb (a), STAR-3 system (b) STAR-4 system (c) and STAR-6 system (d) are formed respectively.

Figure 2: EMUDA constructs of STAR-3 (a), STAR-4 (b) and STAR-6 (c) systems built from dummy atoms 'A' and 'B'.

Figure 3: Off-axis plots showing the Poisson's ratio of the STAR-3 system (a) STAR-4 system (b) and STAR-6 system (c) for $k_h^A, k_h^B \in \left\{50, 800 \text{ kcal mol}^{-1} \text{ rad}^{-2}\right\}$

Figure 4: The deformation mechanism of STAR-3 when $k_h^A = k_h^B = 50 \text{kcal mol}^{-1} \text{ rad}^{-2}$ (a) $k_h^A = 800 \text{kcal mol}^{-1} \text{ rad}^{-2}, k_h^B = 50 \text{kcal mol}^{-1} \text{ rad}^{-2}$ (b), $k_h^A = 50 \text{kcal mol}^{-1} \text{ rad}^{-2}, k_h^B = 800 \text{kcal mol}^{-1} \text{ rad}^{-2}$ (c), $k_h^A = k_h^B = 800 \text{kcal mol}^{-1} \text{ rad}^{-2}$ (d). An animated version of this figure is available in the supplementary information in electronic format.

Figure 5: The deformation mechanism of STAR-4 when $k_h^A = k_h^B = 50 \text{kcal mol}^{-1} \text{ rad}^{-2}$ (a) $k_h^A = 800 \text{kcal mol}^{-1} \text{ rad}^{-2}, k_h^B = 50 \text{kcal mol}^{-1} \text{ rad}^{-2}$ (b), $k_h^A = 50 \text{kcal mol}^{-1} \text{ rad}^{-2}, k_h^B = 800 \text{kcal mol}^{-1} \text{ rad}^{-2}$ (c), $k_h^A = k_h^B = 800 \text{kcal mol}^{-1} \text{ rad}^{-2}$ (d). An animated version of this figure is available in the supplementary information in electronic format.

Figure 6: The deformation mechanism of STAR-6 when

$k_h^A = k_h^B = 50\text{kcal mol}^{-1}\text{ rad}^{-2}$ (a) $k_h^A = 800\text{kcal mol}^{-1}\text{ rad}^{-2}, k_h^B = 50\text{kcal mol}^{-1}\text{ rad}^{-2}$ (b),

$k_h^A = 50\text{kcal mol}^{-1}\text{ rad}^{-2}, k_h^B = 800\text{kcal mol}^{-1}\text{ rad}^{-2}$ (c), $k_h^A = k_h^B = 800\text{kcal mol}^{-1}\text{ rad}^{-2}$

(d). An animated version of this figure is available in the supplementary information

in electronic format.

Figure 7: A graphical representation of the way that the various geometric parameters

of the STAR-3 system change when $k_h^A = k_h^B = 50\text{kcal mol}^{-1}\text{ rad}^{-2}$ (a)

$k_h^A = 800\text{kcal mol}^{-1}\text{ rad}^{-2}, k_h^B = 50\text{kcal mol}^{-1}\text{ rad}^{-2}$ (b),

$k_h^A = 50\text{kcal mol}^{-1}\text{ rad}^{-2}, k_h^B = 800\text{kcal mol}^{-1}\text{ rad}^{-2}$ (c), $k_h^A = k_h^B = 800\text{kcal mol}^{-1}\text{ rad}^{-2}$

(d) for the various angles monitored (e).

Figure 8: A graphical representation of the way that the various geometric parameters

of the STAR-4 system change when $k_h^A = k_h^B = 50\text{kcal mol}^{-1}\text{ rad}^{-2}$ (a)

$k_h^A = 800\text{kcal mol}^{-1}\text{ rad}^{-2}, k_h^B = 50\text{kcal mol}^{-1}\text{ rad}^{-2}$ (b),

$k_h^A = 50\text{kcal mol}^{-1}\text{ rad}^{-2}, k_h^B = 800\text{kcal mol}^{-1}\text{ rad}^{-2}$ (c), $k_h^A = k_h^B = 800\text{kcal mol}^{-1}\text{ rad}^{-2}$

(d) for the various angles monitored (e).

Figure 9: A graphical representation of the way that the various geometric parameters

of the STAR-6 system change when $k_h^A = k_h^B = 50\text{kcal mol}^{-1}\text{ rad}^{-2}$ (a)

$k_h^A = 800\text{kcal mol}^{-1}\text{ rad}^{-2}, k_h^B = 50\text{kcal mol}^{-1}\text{ rad}^{-2}$ (b),

$k_h^A = 50 \text{kcal mol}^{-1} \text{ rad}^{-2}, k_h^B = 800 \text{kcal mol}^{-1} \text{ rad}^{-2}$ (c), $k_h^A = k_h^B = 800 \text{kcal mol}^{-1} \text{ rad}^{-2}$

(d) for the various angles monitored (e).

Figure 10: The conventional STAR-4 units with the AAAA quadrilateral highlighted.

Figure 11: The conventional STAR-6 units with the AAAAAA hexagon (a) and the

BBBBBB hexagon (b) highlighted.

1
2
3
4
5
6
7
8
9
10
11
12
13
14
15
16
17
18
19
20
21
22
23
24
25
26
27
28
29
30
31
32
33
34
35
36
37
38
39
40
41
42
43
44
45
46
47
48
49
50
51
52
53
54
55
56
57
58
59
60

ANIMATIONS FOR STAR-n SYSTEMS

- [Fig4a:] STAR-3 with k_a= 50 kcal mol^{-1} rad^{-2}, k_b = 50 kcal mol^{-1} rad^{-2}
- [Fig4b:] STAR-3 with k_a= 800 kcal mol^{-1} rad^{-2} , k_b = 50 kcal mol^{-1} rad^{-2}
- [Fig4c:] STAR-3 with k_a= 50 kcal mol^{-1} rad^{-2}, k_b = 800 kcal mol^{-1} rad^{-2}
- [Fig4d:] STAR-3 with k_a= 800 kcal mol^{-1} rad^{-2} , k_b = 800 kcal mol^{-1} rad^{-2}

- [Fig5a:] STAR-4 with k_a= 50 kcal mol^{-1} rad^{-2} , k_b = 50 kcal mol^{-1} rad^{-2}
- [Fig5b:] STAR-4 with k_a= 800 kcal mol^{-1} rad^{-2} , k_b = 50 kcal mol^{-1} rad^{-2}
- [Fig5c:] STAR-4 with k_a= 50 kcal mol^{-1} rad^{-2} , k_b = 800 kcal mol^{-1} rad^{-2}
- [Fig5d:] STAR-4 with k_a= 800 kcal mol^{-1} rad^{-2} , k_b = 800 kcal mol^{-1} rad^{-2}

- [Fig6a:] STAR-6 with k_a= 50 kcal mol^{-1} rad^{-2} , k_b = 50 kcal mol^{-1} rad^{-2}
- [Fig6b:] STAR-6 with k_a= 800 kcal mol^{-1} rad^{-2} , k_b = 50 kcal mol^{-1} rad^{-2}
- [Fig6c:] STAR-6 with k_a= 50 kcal mol^{-1} rad^{-2} , k_b = 800 kcal mol^{-1} rad^{-2}
- [Fig6d:] STAR-6 with k_a= 800 kcal mol^{-1} rad^{-2} , k_b = 800 kcal mol^{-1} rad^{-2}